$BiFeO_3$ Films under Tensile Epitaxial Strain from First Principles

B. Dupé,[1] S. Prosandeev,[2] G. Geneste,[3] B. Dkhil,[1] and L. Bellaiche[2]

[1]*Laboratoire Structures, Propriétés et Modélisation des Solides, CNRS-UMR 8580, Ecole Centrale Paris, Grande Voie des Vignes, 92295 Châtenay-Malabry Cedex, France*

[2]*Institute for Nanoscience and Engineering and Physics Department, University of Arkansas, Fayetteville, Arkansas 72701, USA*

[3]*CEA, DAM, DIF, F-91297 Arpajon, France*

(Received 21 January 2011; published 10 June 2011)

Density-functional calculations are performed to predict structural and magnetic properties of (001) $BiFeO_3$ films under tensile epitaxial strain. These films remain monoclinic (Cc space group) for misfit strains between 0% and $\approx 8\%$, with the polarization, tilt axis and magnetization all rotating when varying the strain. At a tensile strain $\approx 8\%$, these films undergo a first-order phase transition towards an orthorhombic phase ($Ima2$ space group). In this novel phase, the polarization and tilt axis lie in the epitaxial plane, while the magnetization is along the out-of-plane direction and the direction of the antiferromagnetic vector is unchanged by the phase transition. An unexpected additional degree of freedom, namely, an antiphase arrangement of Bi atoms, is also found for all tensile strains.

DOI: 10.1103/PhysRevLett.106.237601 PACS numbers: 77.55.Nv, 75.50.Ee, 77.80.bn, 77.84.Bw

Multiferroic compounds are very challenging and fascinating systems in which several order parameters (polarization, strain, magnetism, tilting of oxygen octahedra, etc.) coexist and exhibit subtle interplays [1]. Among multiferroic materials, $BiFeO_3$ (BFO) is unique because it exhibits both ferroelectricity (polar order) and antiferromagnetism (magnetic order) at room temperature, making it a potential candidate for various applications in spintronics [2].

In its bulk rhombohedral $R3c$ ground state, BFO possesses a large polarization $\approx 90\ \mu C/cm^2$ along the pseudocubic [111] direction, coupled to strong antiferrodistortive (AFD) motions about the same axis [3]. The magnetic structure of BFO systems is rather complex. As a matter of fact, the long-period cycloidal spin modulation existing in the bulk [4,5] disappears in epitaxial films [6–8] in favor of a canted spin-configuration in which a strong G-type antiferromagnetism coexists with a weak ferromagnetism. In most potential devices, BFO would be epitaxially grown as a thin film, therefore experiencing a compressive or tensile strain arising from the substrate. Interestingly, theoretical and experimental studies have recently evidenced many unexpected features in compressively strained (001) BFO films. Remarkable examples include the following: (i) a decrease of the Curie temperature with the magnitude of the strain [9] that contrasts with the case of ''classical'' ferroelectrics such as $BaTiO_3$ [10–12]. This decrease was attributed to a strain-induced competition between the polarization and the oxygen octahedra tilts. (ii) A phase transition for misfit strains $\approx -5\%$ showing that BFO can sustain rather large misfit strain, leading to the appearance of a novel phase having high tetragonality ($c/a \approx 1.23$ or more) [13–16] (note also that magnetoelectric coefficients are dramatically enhanced just before this transition [17,18]). While the last years' efforts were concentrated on the compressive strain effects, surprisingly, the tensile part of the phase diagram of BFO films remains mostly unexplored [9,19] despite the possibility of discovering new phenomena. The aim of this Letter is to explore the tensile part of the phase diagram of (001) BFO films by using first-principles calculations. In particular, a novel strain-induced orthorhombic phase accompanied by the occurrence of a giant polarization and a spin-flip of the magnetization is found at high misfit strain. Another order parameter is also discovered for all nonzero tensile misfit strains, in addition to polarization, oxygen octahedra tiltings, antiferromagnetic vector and magnetization. Such order parameter is associated with peculiar in-plane antiphase displacement of Bi atoms.

We have performed density-functional calculations within the local spin density approximation (LSDA), using the SIESTA [20,21] (with Troullier-Martins pseudopotentials) and VASP [22–25] (in the projector augmented wave formalism) codes. Moreover, and as done in Refs. [15–17], the only difference we assume compared to the simulation of a BFO bulk is that in epitaxial (001) BFO films, some components of the strain tensor, $\{\eta\}$, are frozen, while the others are relaxed. More precisely, mechanical boundary conditions of this film are mimicked by imposing that (in the basis for which the x, y, and z axis lie along the pseudocubic [100], [010], and [001] directions, respectively) $\eta_{xy} = \eta_{yx} = 0$ and $\eta_{xx} = \eta_{yy} = \delta$, with δ being the value forcing the film to adopt the in-plane lattice constant of the substrate [10–12]. The various configurations are optimized by making the σ_{zz}, σ_{xz}, σ_{zx}, σ_{yz}, and σ_{zy} components of the stress tensor as well as the atomic forces vanish. σ_{xx}, σ_{yy}, σ_{xy}, and σ_{yx} are thus nonzero and characterize the epitaxial stress. The reference for the calculation of the diagonal components of the strain tensor η_{xx} and η_{yy} is the lattice constant of bulk rhombohedral BFO in the LSDA approximation. Technically, we employ

a 20-atom supercell with a unit cell being doubled along the z direction and rotated by 45° in-plane (in terms of the pseudocubic cell of BFO), in which a G-type antiferromagnetism is enforced. Different configurations, corresponding to different epitaxial strains ranging between 0% and +11.5%, are first optimized using the SIESTA code using a collinear magnetism scheme. These calculations allow us to extract many physical quantities such as the total energy profile, the polarization, the antiferrodistortive angles and the stress, as a function of epitaxial strain [26]. For each simulated δ strain, the ground state structure predicted with the SIESTA code is then used as an input of additional calculations, that are performed with the VASP code and that include noncollinear magnetism and spin-orbit coupling. These latter simulations allow us to predict, for a given direction of the antiferromagnetic vector, the magnitude and direction of the magnetization (if any).

At this point we emphasize that, above misfit strains of a few percent, BFO films can exhibit strain relaxation through interface dislocations or microcracks. However, such relaxation occurs above a given thickness. It is also important to realize that, in the compressive part of the phase diagram, BFO films have been grown without strain relaxation (at least for films of several tens of nanometers) up to large compressive strains of $\approx -4.5/5\%$ on $LaAlO_3$ substrates [16], and even of the order of -7% in the case of $YAlO_3$ substrates [14]. BFO is thus, from this point of view, very unusual. This is probably due to the complex interplay between ferroelectric and AFD degrees of freedom, that coexist in BFO, and that dramatically vary with strain, allowing the appearance of new local minima with different equilibrium lattice constants. Moreover, new phases predicted at high tensile strain at $T = 0$ K can usually be observed at lower strain but for finite temperature [10,12]. Such considerations justify our study of BFO films up to large misfit strain.

Figure 1 gathers the structural, polar and magnetic properties of BFO films under tensile strain up to 11.5%. A clear phase transition occurs around $\delta \approx 8\%$, that we will discuss later. Let us first focus on the misfit strain region for which $\delta \leq 8\%$. Figure 1 indicates that, in this region, the optimized structure is monoclinic and belongs to the Cc space group that is naturally expected from the epitaxy of the bulk rhombohedral $R3c$ structure on a cubic substrate. Interestingly, the same space group is found in the compressive part between 0% and $\approx -5\%$ [9,13–17]. However, for δ ranging between 0% and $\approx 8\%$, the out-of-plane component of the polarization decreases continuously with the strain magnitude whereas its in-plane component increases, while opposite behaviors were found for the compressive region of the Cc space group. As a consequence, the polarization **P** globally increases in magnitude and continuously rotates by bending towards the epitaxial plane (from $\approx 35°$ to 15°), as the tensile strain increases from 0% to $\approx 8\%$ [Fig. 1(a)]. Let us now take a look at the AFD vector, defined such as its direction characterizes the axis about which the oxygen octahedra

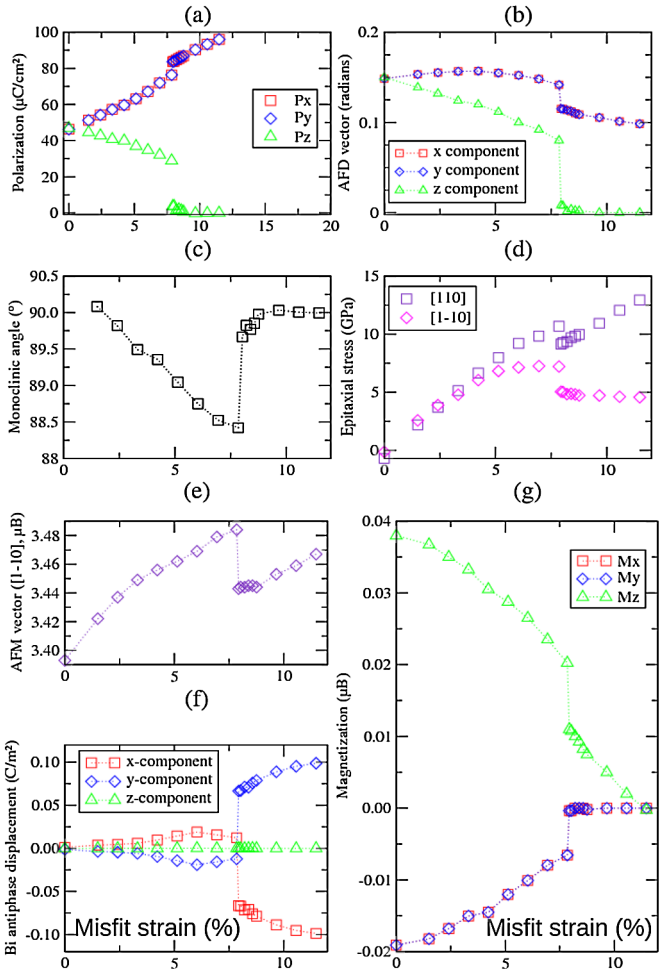

FIG. 1 (color online). Physical properties of (001) BFO films as a function of tensile misfit strain. Panel (a) shows the polarization in $\mu C/cm^2$, while panel (b) displays the AFD vector in radians. Panels (c) and (d) represent the monoclinic angle and epitaxial stress, respectively. Panel (e) shows the magnitude of the antiferromagnetic vector, while panel (g) displays the magnetization (for the most stable direction of the antiferromagnetic vector, i.e., $[1\bar{1}0]$). These magnetic moments are expressed in Bohr magneton per Fe atom. Panel (f) displays the x, y, and z components of the order parameter quantifying the Bi antiphase displacements.

tilt, while its magnitude corresponds to the angle of such tilt. Figure 1(b) shows that the in-plane x and y components of the AFD vector remain quasiconstant ≈ 0.15 radians (8.6°) whereas its z component is linearly reduced with strain by up to $\approx 50\%$ in the tensile part of the Cc phase. The axis about which the oxygen octahedra tilt thus also rotates when varying the tensile strain. Furthermore, the monoclinic angle that is a characteristic of this Cc state decreases from $\approx 90.5°$ to 88.5° [Fig. 1(c)]. Interestingly, a peculiar additional displacement pattern—that is absent at 0% misfit strain—is further observed in this Cc phase. It corresponds to nearest-neighbor Bi atoms moving in opposite directions, parallel or antiparallel to the $[1\bar{1}0]$ pseudocubic direction. Such Bi antiphase displacements,

that are denoted as BAD in the following, therefore occur within the epitaxial plane and are orthogonal to both the polarization and the AFD vector [27]. We quantify them by computing the order parameter **gp** having the following α Cartesian components: $gp_\alpha = \frac{1}{V}\sum_j Z^*_{Bi,\alpha\alpha}\delta r^{Bi}_{j,\alpha} e^{i\vec{k}_{\vec{R}}.\vec{R}_j}$, where $\vec{R}_j$ locates the center of the jth 5-atom cell, $\vec{k}_{\vec{R}}$ is the R point of the Brillouin zone associated with 5-atom cells, and $\delta r^{Bi}_{j,\alpha}$ is the α-component of the displacement of the Bi atom in the jth 5-atom cell (with respect to a centrosymmetric configuration). Finally, Z^*_{Bi} is the effective charge tensor of Bi atoms and V is the supercell volume. The sum runs over all the 5-atom cells j belonging to the supercell. The evolution of the **gp** vector with respect to misfit strain is shown in Fig. 1(f). One can see that the BAD first increase in magnitude between 0% and $\approx 6\%$ and decreases for higher strain in the *Cc* phase, thus exhibiting a maximum (0.02 $\mathrm{C/m^2}$) at $\approx 6\%$.

In this monoclinic phase, the aforementioned calculations using the VASP code allow us to get insight into magnetism. Practically, for each considered epitaxial tensile strain, the electronic structure was recomputed for three different choices for the direction of the antiferromagnetic (AFM) vector, **L**: along the [110] pseudocubic direction (that precisely coincides with the in-plane component of the polarization **P**), along the $[1\bar{1}0]$ pseudocubic direction (that is still an in-plane direction but that is now perpendicular to the in-plane component of the polarization) and along the (out-of-plane) [001] pseudocubic direction. For any considered tensile strain, the lowest energy is provided when **L** lies along the $[1\bar{1}0]$ easy axis, which is in excellent agreement with the recent measurements of Ref. [19] in (001) BFO films under tensile strain. Based on this experimental evidence, we did not try to set **L** along other directions.

The magnitude of the antiferromagnetic vector and components of the magnetization resulting from a spin canting are shown in Figs. 1(e) and 1(g), respectively, (when **L** lies along $[1\bar{1}0]$). The magnitude of **L** only slightly increases with the tensile strain in the *Cc* phase. On the other hand, the weak magnetization significantly decreases its magnitude at the same time [Fig. 1(g)], as a result of the fact that this weak magnetization is driven by the coupling between magnetism and oxygen octahedra tiltings [7,8], and that these tilts are decreasing in magnitude when increasing the strength of the tensile strain; see Fig. 1(b). More importantly, Fig. 1(g) reveals that the magnetization rotates from a $[\bar{1}\,\bar{1}\,2]$ to a $\approx [\bar{1}\,\bar{1}\,3]$ pseudocubic direction (Fig. 2), when the tensile strain increases from 0% to $\approx 8\%$. Such rotation occurs in order to allow the magnetization to remain perpendicular to the axis about which the oxygen octahedra tilt for any tensile strain in the *Cc* state.

One additional and important information revealed by Figs. 1 is that (001) BFO films undergo a first-order strain-driven phase transition from the monoclinic *Cc* phase to an orthorhombic *Ima*2 phase for $\delta \approx 8\%$. In this novel latter phase, both the polarization and the AFD vector lie in the epitaxial plane along the same [110] direction. We are not aware of any previous finding reporting the existence of a *Ima*2 state in BFO films [28]. In this newly discovered orthorhombic phase, the polarization reaches very high values ≈ 120–$130\ \mu\mathrm{C/cm^2}$ that further increase with the tensile strain. On the other hand, the oxygen octahedra tiltings become weaker [Fig. 1(b)], which therefore results in the reduction of the magnitude of the magnetization [Fig. 1(g)]. Note that the most stable direction for the antiferromagnetic vector in the *Ima*2 phase is still the easy $[1\bar{1}0]$-axis, as in the *Cc* state. Interestingly, the magnetization arising from the spin canting has now suddenly moved to be along the out-of-plane [001] direction at the *Cc*-to-*Ima*2 transition as shown schematically in Fig. 2, in order to remain perpendicular to the AFD vector. The spin-flip of the magnetization towards the [001] pseudocubic direction, in addition to the structural and polar softness during this phase transition, may result in huge magnetoelectric effects [17,18]. This phase transition is also numerically found [see Fig. 1(d)] to induce a strong relaxation of the epitaxial stress since $([\sigma_{[110]} + \sigma_{[1\bar{1}0]}]/2$ discontinuously jumps from ≈ 9 GPa to ≈ 7 GPa). This discontinuity confirms the first-order character of this transition (note that a strong first-order phase transition also occurs at the ferroelectric-to-paraelectric phase transition in bulk BFO with a strong variation of the volume of the order of 1.4% [30]). Interestingly, the BAD are also

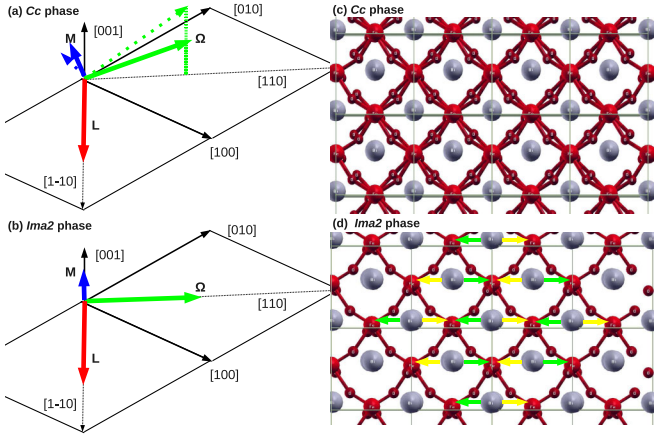

FIG. 2 (color online). Left panel: schematic view of the AFD vector Ω, AFM vector **L** and magnetization **M** in the two phases found in the present work: (a) *Cc* phase; (b) *Ima*2 phase. In panel (a), the solid and dashed arrows are related to two different tensile strain region (low strain in the dashed case, higher strain in the solid case). Right Panel: top view ([001] axis perpendicular to the picture) of these two phases. (c) *Cc* monoclinic phase (tensile strain smaller than $\approx 8\%$), with the oxygen octahedra tilting around [001], as well as, the ferroelectric distortions (in-plane component of the polarization, i.e., along the pseudocubic [110] direction) being clearly visible. (d) *Ima*2 orthorhombic phase (tensile strain larger than $\approx 8\%$), with the strong ferroelectric distortions being clearly visible, as well as the Bi antiphase displacements (that also exist in the *Cc* phase). The yellow and green arrows feature these Bi motions in two consecutive planes perpendicular to the out-of-plane direction.

significant in the *Ima*2 phase [see Fig. 2(d)], with each component of **gp** changing its sign at the phase transition [see Fig. 1(f)].

Among substrates favorable to the appearance of this orthorhombic phase, one might think of alkaline-earth oxides with rocksalt structure. Also, this new phase is likely to occur at smaller misfit strain at finite temperature, since novel phases usually appear at smaller strain when the temperature is increased, as can be inferred for instance from the temperature-misfit strain diagram of standard ferroelectrics such as barium titanate [10,12]. This novel orthorhombic phase possesses similarities with the high-tetragonality phase that has been found in the highly compressive part of the phase diagram of (001) BFO film [13–17]: indeed, the oxygen octahedra are strongly distorted as shown in Fig. 2 with four Fe-O bonds being similar and relatively short while two Fe-O bonds being strongly stretched in-plane (in the compressive part, only one Fe-O bond is strongly elongated out-of-plane). For instance, at 9.66% misfit strain, the short Fe-O distances are 1.94 (in-plane), 1.94 (in-plane), 1.89 (out-of-plane), and 1.89 Å (out-of-plane) while the two other Fe-O distances (that are in-plane) are 2.44 Å. These strong ferroelectric distortions are responsible for the large value of the (in-plane) polarization in this orthorhombic phase.

In this work, we have studied, from first-principles, structural, polar and magnetic properties of (001) BFO films under tensile epitaxial strain. We have found that these important materials (i) remain in a monoclinic *Cc* phase exhibiting oxygen octahedra tilts and nonzero components of the polarization along x, y, and z between 0 and $\approx 8\%$, with both the axis about which the oxygen octahedra tilt and the polarization rotating with the magnitude of the strain, (ii) undergo a first-order phase transition, at $\delta = 8\%$, towards a novel orthorhombic phase of *Ima*2 space group in which the tilts and the polarization have no out-of-plane components, and (iii) exhibit an antiphase Bi displacement pattern in both the *Cc* and *Ima*2 phases. For all investigated tensile strains, the antiferromagnetic vector is found to be the most stable along an in-plane $[1\bar{1}0]$ direction, among three directions tested ($[1\bar{1}0]$, [110], and [001]). This allows **L** to remain perpendicular to both the polarization and AFD vector for any strain. Moreover, the *Cc* and *Ima*2 phases both exhibit a weak ferromagnetic vector (coming from a spin canting), with this vector rotating and decreasing in magnitude with strain in the *Cc* state while it flips along the out-of-plane direction in the *Ima*2 phase. In other words, tensile strain not only controls the direction and magnitude of several structural order parameters, but also affects the direction and magnitude of magnetization. Some magnetoelectric coefficients may thus be dramatically modified by tensile strains in (001) BFO films. We hope that our study is of large benefits to the active research fields of multiferroics and nanoscience.

We thank I. A. Kornev for useful discussions. L. B. and S. P. thank the support of ONR grants N00014-08-1-0915 and N00014-07-1-0825 (DURIP). DOE under contract ER-46612 and NSF grantsDMR-0701558 and DMR-0080054 are also acknowledged for discussion with scientists sponsored by these grants.

[1] G. A. Smolenskii and I. E. Chupis, Sov. Phys. Usp. **25**, 475 (1982).
[2] G. Catalan and J. F. Scott, Adv. Mater. **209**, 1 (2009).
[3] J. B. Neaton *et al.*, Phys. Rev. B **71**, 014113 (2005).
[4] I. Sosnowska *et al.*, Physica (Amsterdam) **180–181B**, 117 (1992).
[5] D. Lebeugle *et al.*, Phys. Rev. Lett. **100**, 227602 (2008).
[6] H. Bea *et al.*, Appl. Phys. Lett. **87**, 072508 (2005); H. Bea *et al.*, Philos. Mag. Lett. **87**, 165 (2007).
[7] C. Ederer and N. A. Spaldin, Phys. Rev. B **71**, R060401 (2005).
[8] D. Albrecht *et al.*, Phys. Rev. B **81**, 140401(R) (2010).
[9] I. C. Infante *et al.*, Phys. Rev. Lett. **105**, 057601 (2010).
[10] N. A. Pertsev, A. G. Zembilgotov, and A. K. Tagantsev, Phys. Rev. Lett. **80**, 1988 (1998).
[11] O. Diéguez, K. M. Rabe, and D. Vanderbilt, Phys. Rev. B **72**, 144101 (2005).
[12] B.-K. Lai, I. A. Kornev, L. Bellaiche, and G. J. Salamo, Appl. Phys. Lett. **86**, 132904 (2005).
[13] H. Béa *et al.*, Phys. Rev. Lett. **102**, 217603 (2009).
[14] R. J. Zeches *et al.*, Science **326**, 977 (2009).
[15] A. J. Hatt, N. A. Spaldin, and C. Ederer, Phys. Rev. B **81**, 054109 (2010).
[16] B. Dupé *et al.*, Phys. Rev. B **81**, 144128 (2010).
[17] J. C. Wojdel and J. Íñiguez, Phys. Rev. Lett. **105**, 037208 (2010).
[18] S. Prosandeev, I. A. Kornev, and L. Bellaiche, Phys. Rev. B **83**, 020102(R) (2011).
[19] M. B. Holcomb *et al.*, Phys. Rev. B **81**, 134406 (2010).
[20] P. Ordejon, E. Artacho, and J. M. Soler, Phys. Rev. B **53**, R10441 (1996).
[21] J. M. Soler *et al.*, J. Phys. Condens. Matter **14**, 2745 (2002).
[22] G. Kresse and J. Hafner, Phys. Rev. B **47**, 558 (1993); **49**, 14 251 (1994).
[23] G. Kresse and J. Furthmuller, Comput. Mater. Sci. **6**, 15 (1996).
[24] G. Kresse and J. Furthmuller, Phys. Rev. B **54**, 11 169 (1996).
[25] G. Kresse and D. Joubert, Phys. Rev. B **59**, 1758 (1999).
[26] We also performed LSDA + U calculations with $U =$ 3.87 eV, using the VASP code [22–25]. Such additional computations qualitatively agree with the LSDA results reported here for all investigated tensile strains.
[27] These Bi antiphase displacements also exist in the *Cc* phase under compressive strain. They have been overlooked in all the previous works dedicated to (001) BFO films, to the best of our knowledge.
[28] Note that, on the other hand, a *Ima*2 phase has been predicted to occur in Ref. [29] in BFO bulk being under an electric field oriented along the pseudocubic $[\bar{1}\,\bar{1}\,0]$ direction and for a narrow range of field's magnitude.
[29] S. Lisenkov, D. Rahmedov, and L. Bellaiche, Phys. Rev. Lett. **103**, 047204 (2009).
[30] R. Haumont *et al.*, Phys. Rev. B **78**, 134108 (2008).